A numerical study on the effective thermal conductivity of biological fluids containing single-walled carbon nanotubes

Hai M. Duong[1], Dimitrios V. Papavassiliou[2], Kieran J. Mullen[3], Brian L. Wardle[4] and Shigeo Maruyama[1*]

[1]Department of Mechanical Engineering, The University of Tokyo, Japan
[2]School of Chemical, Biological and Materials Engineering, The University of Oklahoma, USA
[3]Department of Physics and Astronomy, The University of Oklahoma, USA
[4]Department of Aeronautics and Astronautics, Massachusetts Institute of Technology, USA

Abstract

Thermal death of cancerous cells may be induced by radiating single-walled carbon nanotubes (SWNTs) selectively attached via functionalization to the targeted cells. A distribution of SWNTs inside cancerous cells, on their surface, or in the inter-cellular fluid may occur during this treatment process. This work applies a random walk algorithm to calculate the effective thermal conductivity of an idealized biological fluid containing SWNTs. The thermal resistance at the interface between the SWNTs and their surroundings is incorporated to make predictions that are required for developing an overall approach to cancerous cell targeting.

---

* Corresponding author. TEL: +81 3 5841 6421; FAX : +81 3 5800 6983. Email: maruyama@photon.t.u-tokyo.ac.jp

Key words: SWNT, thermal boundary resistance, thermal conductivity, radiation therapy

Nomenclature

A_c surface area of a SWNT, cm^2

C blood density, g/cm^3

C_f thermal equilibrium factor

C_m sound velocity in blood, m/s

C_p specific heat of blood, kJ/kg K

D diameter of a SWNT, nm

D_b thermal diffusivity of blood, cm^2/s

$f_{b\text{-}CN}$ probability of a walker moving into the SWNT phase

$f_{CN\text{-}b}$ probability of a walker crossing into the blood

K_{bd} thermal boundary conductance, MW/ m^2K

K_b thermal conductivity of the blood, W/mK

K_{eff} effective thermal conductivity, W/mK

L length of a SWNT, cm

R_{bd} thermal boundary resistance, m^2K/W

V_c volume of a SWNT, cm^3

Greek symbols

Δt time increment, ns

λ wavelength, nm

ρ blood density, g/cm^3

σ standard deviation, cm

1. Introduction

Single-walled carbon nanotubes (SWNTs) have excellent electrical, thermal and mechanical characteristics [1-3]. Of particular promise are recent findings that SWNTs

can transport various molecules across the cellular membrane without cytotoxicity [4-6]. Quite notably, a test of carbon nanotubes administered to mice intravenously in the form of a water solution (0.5 g/l of SWNTs and multi-walled carbon nanotubes (MWNTs) in water) indicated that such carbon nanotubes may be safe to use in the body [7]. Functionalized carbon nanotubes can circulate in the blood of live animals and can be removed from the blood system through processing in the kidneys and excretion in urine [7].

Kam *et al.* [8] suggested that if SWNTs can be selectively internalized into cancer cells with specific tumor markers, the near infrared radiation (NIR) to the nanotubes in vitro can then selectively trigger thermal cell death without harming normal cells. Another option is to attach functionalized nanotubes on the surface of cancer cells using proteins that attach selectively to the membrane of malignant cells (fig. 1(a)). In current practice, radiation cannot selectively target individual tumor cells and, thus, normal cells within the radiation field suffer damage, leading to potentially serious side effects. However, the radiation can be controlled by using internal images to guide focused beams. Controlled cell destruction could be achieved by functionalized SWNTs that attach selectively to cancerous cells. (For example, exposure of phosphatidylserine occurs on the surface of cancerous cells, but not on the surface of healthy cells [9]. Appropriately functionalized nanotubes could therefore be attached at a high concentration on the surface of such cells. Another example is that SWNTs can be selectively internalized by cells labeled with folate receptor tumor markers [10]). Kam *et al.* [8] demonstrated that SWNTs exhibit very high optical absorbance in the NIR regime where biological systems are transparent with a laser of wavelength λ = 808 nm. While biological systems are transparent to 700-1100 nm NIR [11], the SWNTs with appropriate diameter absorb strongly in this window [12] and they can potentially be used for optical stimulation inside or outside living cells to afford various useful functions. Continuous NIR radiation, however, can cause cell death because of excessive local heating of SWNTs *in vitro*. The efficient *in vitro* excitations of SWNTs depend on their chirality, orientation and quantity to obtain enhanced biological effects [8].

In order to understand how best to develop this technique, it will be necessary to model the deposition and subsequent dissipation of heat in the system. This will require

knowledge of the thermal conductivity of the cancer cells when loaded with SWNTs, of the normal cells, and of the inter-cellular fluid. The transfer of heat from NIR-stimulated SWNTs to the surrounding biological fluid (like blood) is affected by the thermal boundary resistance that exists at the interface between SWNTs and any medium in contact with the SWNTs. The thermal properties of SWNTs in blood, for example, are characterized by an *effective thermal conductivity* of the SWNTs that accounts for the intrinsic thermal conductivity of the SWNTs as well as the thermal boundary resistance of the SWNT-blood juncture, instead of the nominal thermal conductivity. The goal of this study is to investigate the role of thermal boundary resistance on effective thermal conductivity of SWNTs dispersed in aqueous environments such as those characteristic of biological fluids. This will enable future modeling of specific irradiation approaches.

2. Simulation Methodology

The random walk algorithm developed by Duong *et al.* [13,14] for conductive heat transport is applied. This off-lattice Monte Carlo algorithm is an improvement of previous computational models [15-16] and has been validated with experimental data for SWNT-polymer composites [13]. Figure 1 is a conceptual diagram of the SWNTs concentrated around a cell and the configuration of the SWNTs in the simulation. The modeling focuses on the effective thermal properties of SWNTs in the blood medium that is critical in predicting the effectiveness requirements of the SWNT functionalization. The computational domain is a cube (96 x 96 x 96 bin^3) or a rectangle (288 x 96 x 96 bin^3) depending on the aspect ratio *L/D* and having SWNTs dispersed into a fluid that has macroscopic properties equal to those of blood. The computational domain is heated from one surface (the $x = 0$ plane) with the release of 90,000 thermal walkers distributed uniformly on that surface. The walkers exit at the surface opposite to the heated plane. The cell is periodic in the other two directions. The computation of the effective transport coefficients is based on the simulation of the trajectories of the walkers traveling through a computational cell for a long enough time. The adequacy of the number of walkers, and of the size of the computational domain, for the calculation of the effective thermal conductivity has been discussed elsewhere [14]. The temperature distribution is

calculated from the number of walkers found in each bin. The walkers move through the fluid by Brownian motion [17] whose model has been used successfully to simulate heat transfer due to diffusion in the case of convective flows [18-20]. The Brownian motion in each space direction is simulated with random jumps that each walker executes at each time step. These jumps take values from a normal distribution with a zero mean and a standard deviation

$$\sigma = \sqrt{2D_b \Delta t} \tag{1}$$

where D_b is the thermal diffusivity of the blood and Δt is the time increment.

Once a walker in the blood reaches the interface between the blood and a SWNT, the walker will move into the SWNT phase with a probability $f_{\text{b-CN}}$, which represents the thermal resistance of the interface and will stay at the previous position in the matrix with a probability $(1\text{-}f_{\text{b-CN}})$. Similarly, once a walker is inside a SWNT, the walker distributes randomly within the SWNT due to the high SWNT thermal conductivity with a probability $(1\text{-}f_{\text{CN-b}})$ at the end of a time step, and will cross into the blood with a probability $f_{\text{CN-b}}$. The carbon nanotube thermal conductivity is treated as effectively infinite. With this approximation in the model, the aspect ratio of the nanotube becomes important as higher aspect ratios (longer nanotubes) amplify the effect of this assumption of relative conductance of the SWNTs vs. the matrix. Thermal boundary resistance thus becomes appropriately emphasized at the SWNT-matrix interface. In this latter case, the walker moves first to a random point anywhere on the surface of the SWNT and then moves with a normal distribution into the matrix. The thermal boundary resistance is the same for the walker coming in and out the SWNTs and for SWNT walls and ends. The thermal resistance is the same when a walker moves from one phase into the other, but this does not mean that $f_{\text{b-CN}} = f_{\text{CN-b}}$. In thermal equilibrium, the average walker density within the SWNTs should be equal to that in the surrounding fluid. As the walkers can leave anywhere on the surface the next time step, the exit probability $f_{\text{CN-b}}$ must be weighted so that the flux of walkers into the SWNTs equals that going out when they are in equilibrium. The weight factor depends only upon geometry, and to maintain equilibrium the two probabilities are related as

$$f_{CN-b} = C_f \frac{\sigma A_c}{V_c} f_{b-CN} \tag{2}$$

where A_c and V_c are the surface area and the volume of a SWNT, respectively; σ is the standard deviation of the random jump in the blood and C_f is the thermal equilibrium factor. The thermal equilibrium factor C_f of the SWNTs used in this work has been determined by numerical trial and error [13] to be 0.25. The purpose of the C_f is to recover a length scale in the problem (i.e., A_c/V_c) that is lost when the thermal walkers are assumed to be uniformly distributed inside the SWNTs, instead of moving with random steps obtained from a normal distribution.

The calculation of the effective conductivity is simplified by simulating heat transfer with constant heat flux through the domain with hot and cold opposite planes releasing `hot` and `cold` walkers (carrying negative energy), respectively. More details about the random walk algorithm can be found in Duong *et al*. [13, 14].

Further assumptions in the model are that SWNTs are dispersed without forming bundles and the transfer of heat is passive (i.e., the thermal conductivity or the density of the fluid does not change during the process). Furthermore, the functionalization of the SWNTs is taken into account by varying the thermal boundary resistant values ($f_{b\text{-}CN}$ changes) as far as the heat transfer behavior is concerned. The transfer of heat from the SWNTs to the cell surface (see Figure 1) is expected to happen by conduction only, since the fluid between the nanotubes and the cell is expected to be stationary relative to the cell and the nanotubes.

Heat transfer, as described above, was studied in a computational cell containing 2.40 nm-diameter SWNTs [21] with different lengths. Typical diameters, *D*, of experimentally available SWNTs are 1.0-1.5 nm, when they are grown by laser-furnace [22] and arc-discharge [23] growth techniques, and are 0.7- 3.0 nm when grown by CVD techniques [24-26]. The length, *L*, of 'as-grown' SWNTs is usually longer than several micrometers, but it can be shortened to several hundreds of nanometers through purification and dispersion processes. Hence, the aspect ratio *L/D* could be up to 1,000. Choosing the proper aspect ratio *L/D* for the simulations is essential, as the computational domain cell and the simulation time are limited. Based on the effective medium theory [13], the effects of the aspect ratio on the effective thermal conductivity are negligible once *L/D* is larger than a critical value. According to a numerical investigation utilizing the algorithm implemented here, Duong *et al.* [27] found that *L/D* =120 is large enough

to assume that larger *L/D* will not have a significant effect on the results. In the simulations conducted herein, aspect ratios of *L/D* = 40 and 120 were chosen, and the SWNT diameter was set to be *D* = 2.40 nm. Depending on the weight fraction of SWNTs, the number of SWNTs in the cubic cell varied from 31 to 495. The model of 60 SWNTs in blood with a weight fraction of 0.1 % and L/D = 40 is shown in Figure 1. The SWNTs were randomly dispersed, perpendicular or parallel to the direction of heat flow (i.e, the x-axis) with random locations of SWNTs in all cases.

The exact thermal resistance of the SWNT-blood interface is difficult to predict, and it depends strongly on the chemical composition of the fluid surrounding a SWNT. Since over 50% of blood is in fact water, and since the fluid environment inside cells is essentially an aqueous environment, we assume that the interfacial resistance to heat transfer will be that of a SWNT-water interface, or, at least, it will have a value very close to that. Maruyama *et al.* [28] conducted molecular dynamic simulations to calculate the thermal boundary resistance between a (10,10) SWNT and water. The simulated SWNT contained 192 water molecules inside its hollow space. The thermal boundary resistance, R_{bd} was estimated to be 2.0×10^{-7} m^2K/W (corresponding to a thermal boundary conductance, K_{bd} = 5 MW/m^2K). Huxtable *et al.* [29] used picosecond transient adsorption to measure the interface thermal conductance of carbon nanotubes suspended in surfactant micelles in water. Their experimental results showed that the interface thermal resistance was 0.84×10^{-7} m^2K/W (K_{bd} = 12 MW/m^2K). Since the enhancement of effective thermal conductivities was relatively small for these reasonable thermal boundary resistances and reasonable weight fractions of SWNTs, we further studied a range of low thermal resistance, R_{bd} = 0.005, 0.010, 0.025 and 0.250 [10^{-7} m^2K/W] (K_{bd} = 2000, 1000, 400 and 40 MW/m^2K, respectively). The weight fraction of SWNTs was determined to be in the range of the weight fraction reported in experiments of stabilizing nanotube suspensions with proteins [7,8,30] and above (0.1 wt%, 0.5 wt% and 1.0 wt%). These values could be appropriate for concentrated SWNTs on the surface of a cell. Since the exact configuration of the SWNTs when they are attached to a cell surface is not presently known, and since there is a strong possibility that SWNTs can be oriented in preferential directions, the simulations have covered the case that the heat flux is parallel

or perpendicular to the SWNT axis, as well as the case of random SWNT orientation relative to the heat flux direction.

3. Results and Discussion

3-1. Thermal boundary resistance equivalent to water suspension

A summary of parameters used in the simulations is given in Table 1. The effective thermal conductivity of SWNTs in blood is shown in Figure 2 using the two different thermal boundary resistances reported for SWNTs and water ($R_{bd} = 0.84 \times 10^{-7}$ and 2.0×10^{-7} m^2K/W or $K_{bd} = 12$ and 5 MW/m^2K, respectively), with different weight fractions of SWNTs (0.05, 0.075 and 0.1 wt% or 31, 46 and 60 SWNTs), different orientation (SWNTs are parallel and perpendicular to heat flux or dispersed randomly), and different SWNT length (L/D = 40 and 120). The matrix probabilities, $f_{b\text{-}CN}$ are calculated to be 0.0025 and 0.0060 using the acoustic mismatch theory [31]

$$f_{b-CN} = \frac{4}{\rho C C_m R_{bd}} \tag{3}$$

where ρ is the blood density; C is the blood specific heat and C_m is the velocity of sound in blood.

The simulated ratio of effective thermal conductivities to the pure blood is summarized in Table 2. For the shorter SWNTs in Fig. 2a, the effective thermal conductivity is almost linearly proportional to the weight fraction of SWNTs. This result suggests that the weight fraction is very small so that effect of each SWNT can be independent. The ‘parallel’ and ‘perpendicular’ curves show the maximum and the minimum thermal conductivity of the SWNT-blood systems. The effective thermal conductivity is smaller than the conductivity of pure blood when the SWNTs are perpendicular to the heat flow. This is because the walkers need to stay within SWNTs until they will have a chance to come-out by the probability inversely proportional to the thermal boundary resistance. The reduction of effective thermal conductivity is observed even for randomly dispersed case for larger thermal boundary resistance for L/D = 40 in Fig. 2a.

The effective thermal conductivities are larger for longer SWNTs as shown in Fig. 2b. The dependency on the SWNT weight fractions is no longer linear within 0.1 wt % for L/D = 120. Because of the length of SWNTs, effective thermal conductivity increases for randomly dispersed case even with large thermal boundary resistance.

By controlling the functionalization of SWNTs, the orientation of SWNTs outside the cancer cells could be controlled. Therefore, the thermal conductivities of the SWNTs in the blood can reach a maximum if the dispersed SWNTs are oriented parallel to the heat flux. The simulation results show that for up to 0.1% of weight fraction of the SWNTs the thermal conductivities of SWNTs perpendicular to the heat flux are less affected by thermal boundary resistance. The effective thermal conductivities are lower than that of the pure blood, and decrease when the weight fraction of SWNTs increases. When short SWNTs are dispersed randomly in the blood, the thermal conductivities are not enhanced much – the maximum conductivity is increased by only 0.6% at 0.1% of weight fraction of SWNTs (Figure 2a). This can be explained because the quantity of SWNTs is small and the thermal boundary resistance values used is high, so that the walkers cannot cross into the SWNTs and travel faster. The effective thermal conductivity can be significantly enhanced only when the SWNT orientation can be controlled. For example, when the SWNTs are parallel to the heat flux, the effective thermal conductivity is enhanced by 14% at 0.1 wt% SWNTs in the fluid for L/D = 40. On the other hand, effective thermal conductivity for 'random' is similar to 'parallel' for longer SWNTs (L/D = 120).

3-2. Smaller thermal boundary resistance and larger weight fraction of SWNTs

As the thermal conductivity of the randomly distributed SWNT-blood system is not significantly affected by 0.1 wt% of the SWNTs over the above thermal boundary resistance range ($R_{bd} = 0.84 \times 10^{-7}$ and 2.0×10^{-7} m^2K/W or K_{bd} = 12 and 5 MW/ m^2K), we conducted a systematical study with lower values of the thermal boundary resistance, as shown in Table 3. The thermal boundary resistance between the SWNTs and the blood may be reduced by better controlling the SWNT functionalization processes. Table 3 shows the ratio of the effective thermal conductivities of SWNTs in blood divided by the conductivity of pure blood with constant heat flux. For each kind of SWNT orientation in

the computational cell, and each value of thermal boundary resistance and weight fraction of SWNTs, the thermal conductivity presented is the average of three simulations, each of which conducted with a different distribution of SWNTs in the computational cell.

The effective thermal conductivity of the SWNT blood system increases when the thermal boundary resistance decreases. The dependence of effective thermal conductivities on thermal boundary resistance is plotted in Fig. 3 for 0.1 wt % SWNTs. With increasing thermal boundary conductance, effective thermal conductivities monotonically increase.

Figure 4 shows the effective thermal conductivities for smaller thermal boundary resistances, $R_{bd} = 0.25 \times 10^{-7}$ and 0.01×10^{-7} m^2K/W or $K_{bd} = 40$ and 1000 MW/ m^2K. With the longer SWNT ($L/D = 120$) in Fig. 4b, the effective thermal conductivities of the SWNT blood system are almost the same for the case in which SWNTs are perpendicular to the heat flux and greater for the cases in which SWNTs are dispersed randomly and parallel to the heat flux due to heat transfer along the SWNT axis. With the same thermal boundary resistance and the same L/D ratio, weight fraction, and dispersion pattern of SWNTs, the random jump of walkers in the heat flow direction is less (meaning worse heat transfer) for SWNTs perpendicular to the heat flux, higher for the random distribution of the SWNTs, and maximum for the SWNTs parallel to the heat flux, as expected. With the same thermal boundary resistance and the same L/D ratio, the ratio of the maximum and the minimum thermal conductivity increases when increasing the weight fraction of SWNTs. With the same weight fraction and the same L/D ratio, this effective thermal conductivity ratio decreases if the thermal boundary resistance increases.

Simulation results also show that the thermal conductivity of the SWNT-blood system is smaller than the conductivity of pure blood when the SWNTs are perpendicular to the heat flow and the thermal boundary resistance is high. The presence of SWNTs having very high thermal boundary resistance in the domain inhibits heat transfer (or prevents the walkers traveling forward) in the computational cell. This causes the effective thermal conductivity to be reduced. Once the thermal boundary resistance is very small ($f_{b\text{-}CN}$=1.0), the heat walkers can cross the SWNT-blood interface easily and travel faster along the SWNT radius. So the thermal conductivities increase once the SWNT weight fractions increases in this case as in Table 3.

Figure 5 shows the thermal conductivities of SWNTs dispersed randomly in the blood with different thermal boundary resistance and different L/D ratios. The large increase of effective thermal conductivities for longer SWNTs is apparent from Fig. 5.

The effective thermal conductivity, K_{eff}, is still much lower than that calculated by the modified Maxwell theory for non-spherical inclusions, even in the case of heat transfer with SWNTs oriented parallel to the direction of heat transfer [32]. The thermal conductivity of 0.1 wt% of SWNTs (thermal conductivity in the range 1750-6600 W/m K) in the blood can be calculated to be between ~48.0 – 179.5 W/mK, while the maximum thermal conductivity from the simulation is ~3.7 W/mK, (i.e., ~7.2 times greater than that of the pure human blood, as shown in Table 3 for SWNTs aligned parallel to the direction of heat flux). The higher effective thermal conductivity of SWNT blood system can reduce the impulse time and may not damage the normal cells as the radiation has not been controlled well currently.

4. Conclusions

This study computed the effective thermal conductivities of SWNTs dispersed in an aqueous solution that can represent blood over a range of thermal boundary resistance and SWNT weight fraction. It was found that the effective thermal conductivity of SWNTs in blood is much lower than the value estimated from the Maxwell theory, when taking account of the existence of a thermal boundary resistance. The maximum and minimum possible thermal conductivity has been determined, according to the orientation of the dispersed SWNTs in the biological systems. Even though the analysis presented applies more directly to SWNTs attached externally to the cell membrane, the effective conductivities calculated here for the case of random SWNT orientation could be used in cases of SWNTs internalized into cells, since the fluid environment within cells is aqueous. Given the density profiles of SWNT in cancerous and healthy cells, and in any encompassing medium, we can in the future calculate how energy deposited by NIR will be dissipated in the tissue. This may allow the process to be optimized to do maximum damage to cancer cells and minimum damage to nearby healthy tissue.

Acknowledgments

This work was supported by the National Computational Science Alliance under CTS-040023 and by the TeraGrid under TG-CTS070037T, and it utilized the NCSA IBMp690. We also want to acknowledge useful conversations with Professor R.G. Harrison at the University of Oklahoma. Dimitrios Papavassiliou acknowledges support from the DoE-funded Center for Applications of Single-Walled Carbon Nanotubes – (Award Register#: ER64239 0012293).

References

[1] S. Iijima, T. Ichihashi, Single-shell carbon nanotubes of 1-nm diameter, Nature (London) 363 (1993) 603-605.

[2] D.S. Bethune, C.H. Klang, M.S. De Vries, G. Gorman, R. Savoy, J. Vazquez, R. Beyers, Cobalt-catalysed growth of carbon nanotubes with single-atomic-layer walls, Nature (London) 363 (1993) 605-607.

[3] M. Meyyappan, Carbon Nanotubes Science and Applications, CRC Press, New York, 2005.

[4] A. Bianco, K. Kostarelos, C.D. Partidos, M. Prato, Biomedical applications of functionalised carbon nanotubes, Chem. Commun. 5 (2005) 571-577.

[5] N.W.S. Kam, T.C. Jessop, P.A. Wender, H.J. Dai, Nanotube Molecular Transporters: Internalization of Carbon Nanotube-Protein Conjugates into Mammalian Cells, J. Am. Chem. Soc. 126 (2004) 6850-6851.

[6] P. Cherukuri, S.M. Bachilo, S.H. Litovsky, R.B. Weisman, Near-Infrared Fluorescence Microscopy of Single-Walled Carbon Nanotubes in Phagocytic Cells, J. Am. Chem. Soc. 126 (2004) 15638 -15639.

[7] R. Singh, D. Pantarotto, G. Pastorin, C. Klumpp, M. Prato, A. Bianco, K. Kostarelos, Tissue biodistribution and blood clearance rates of intravenously administered carbon nanotube radiotracers, PNAS 103 (9) (2006) 3357-3362.

[8] N.W.S Kam, M. OConnell, J.A. Wisdom, H.J. Dai, Carbon nanotubes as multifunctional biological transporters and near-infrared agents for selective cancer cell destruction, PNAS 102 (33) (2005) 11600-11605.

[9] S. Ran, A. Downes, P.E. Thorpe, Increased Exposure of Anionic Phospholipids on the Surface of Tumor Blood Vessels, Cancer Research 62 (21) (2002) 6132-6140.

[10] Y.J. Lu, E. Sega, C.P. Leamon, P.S. Low, Folate receptor-targeted immunotherapy of cancer: mechanism and therapeutic potential, Adv. Drug Delivery Rev. 56 (2004) 1161-1176.

[11] K. Konig, Multiphoton microscopy in life sciences, J. Microscopy - Oxford 200 (2000) 83-104.

[12] M.J. O'Connell, S.M. Bachilo, C.B. Huffman, V.C. Moore, M.S. Strano, E.H. Haroz, K.L. Rialon, P.J. Boul, W.H. Kittrell *et al.*, Band Gap Fluorescence from Individual Single-Walled Carbon Nanotubes, Science 297 (2002) 593-596.

[13] M.H. Duong, D.V. Papavassiliou, J.K. Mullen, S. Maruyama, Computational modeling of the thermal conductivity of single-walled carbon nanotube–polymer composites, Nanotechnology, 19 (2008) Art. No 065702 (8pp).

[14] M.H Duong, D.V. Papavassiliou, J.K. Mullen, L.L. Lee, Random walks in nanotube composites: Improved algorithms and the role of thermal boundary resistance, Appl. Phys. Lett. 87 (1) (2005) Art. No 013101 (3pp).

[15] M.M. Tomadakis, S.V. Sotirchos, Transport properties of random arrays of freely overlapping cylinders with various orientation distributions**,** J.Chem.Phys. 98 (1993) 616-626.

[16] M.M. Tomadakis, S.V. Sotirchos, Transport through random arrays of conductive cylinders dispersed in a conductive matrix, J.Chem.Phys. 104 (1996) 6893-6900.

[17] A. Einstein, Ann. Phys. Lpz. 17 (1905) 549.

[18] D.V. Papavassiliou, T.J. Hanratty, Transport of a passive scalar in a turbulent channel flow, Int. J. Heat Mass Transfer 40 (6) (1997) 1303-1311.

[19] B.M. Mitrovic, P.M. Le, D.V. Papavassiliou, On the Prandtl or Schmidt number dependence of the turbulent heat or mass transfer coefficient, Chem. Eng. Sci. 59 (3) (2004) 543-555.

[20] P.M. Le, D.V. Papavassiliou, Turbulent Heat Transfer in Plane Couette Flow, J. Heat Transfer Trans. ASME 128 (2006) 53-62.

[21] Y. Murakami, E. Einarsson, T. Edamura, S. Maruyama, Polarization Dependent Optical Absorption Properties of Single-Walled Carbon Nanotubes and Methodology for the Evaluation of Their Morphology, Carbon 43 (2005) 2664.

[22] A. Thess, R. Lee, P. Nikolaev, D. Dai, P. Petit, J. Robert, C. Xu, Y.H. Lee, S.G. Kim, A.G. Rinzler, D.T. Colbert, G.E. Scuseria, D. Tomanek, J.E. Fischer, R.E. Smalley, Crystalline Ropes of Metallic Carbon Nanotubes, Science 273 (1996) 483-487.

[23] C. Journet, W.K. Maser, P. Bernier, A. Loiseau, M.L. De la Chappelle, S. Lefrant, P. Deniard, R. Lee, J.E. Fischer, Large-scale production of single-walled carbon nanotubes by the electric-arc technique, Nature 388 (1997) 756-758.

[24] P. Nikolaev, M.J. Bronikoski, R.K. Bradley, F. Rohmund, D.T. Colbert, K.A. Smith, R.E. Smalley, Gas-phase catalytic growth of single-walled carbon nanotubes from carbon monoxide, Chem. Phys. Lett. 313 (1999) 91-97.

[25] S. Maruyama, R. Kojima, Y. Miyauchi, S. Chiashi, M. Kohno, Low-temperature synthesis of high-purity single-walled carbon nanotubes from alcohol, Chem. Phys. Lett. 360 (2002) 229-234.

[26] Y. Murakami, S. Chiashi, Y. Miyauchi, M. Hu, M. Ogura, T. Okubo, S. Maruyama, Growth of vertically aligned single-walled carbon nanotube films on quartz substrates and their optical anisotropy, Chem. Phys. Lett. 385 (2004) 298-303.

[27] H.M. Duong, D.V. Papavassiliou, K.J. Mullen, B.L. Wardle, S. Maruyama, The prediction of thermal properties of single walled carbon nanotube suspensions, J. Phys. Chem. C (2008) published online.

[28] S. Maruyama, Y. Igarashi, Y. Taniguchi, J. Shiomi, Anisotropic Heat Transfer of Single-Walled Carbon Nanotubes, J. Therm. Sci. Tech. 1 (2006) 138-148.

[29] S.T. Huxtable, D.G. Cahill, S. Shenogin, L. Xue, R. Ozisik, P. Barone, M. Usrey, M.S. Strano, G. Siddons, M. Shim, P. Keblinski, Interfacial heat flow in carbon nanotube suspensions, Nature Materials 2 (2003) 731-734.

[30] N.R. Palwai, D.E. Martyn, L.F.F. Neves, Y. Tan, D.E. Resasco, R.G. Harrison, Retention of biological activity and near-infrared absorbance upon adsorption of horseradish peroxidase on single-walled carbon nanotubes, Nanotechnology 18 (23) (2007) Art. No 235601 (5pp).

[31] E.T. Swartz, R.O. Pohl, Thermal boundary resistance, Rev. Mod. Phys. 61 (3) (1989) 605-668.

[32] R.B. Bird, W.S. Stewart, E.N. Lightfoot, Transport Phenomena, second ed., John Wiley & Sons Inc., New York, 2002, p.p.282, 376 and 379.

[33] V.M. Nahirnyak, S.W. Yoon, C.K. Holland, Acousto-mechanical and thermal properties of clotted blood, The Journal of the Acoustical Society of America 119 (6) (2006) 3766-3772.

[34] G.R. Lockwood, L.K. Ryan, J.W. Hunt, F.S. Foster, Measurement of the ultrasonic properties of vascular tissues and blood from 35–65 MHz, Ultrasound Med. Bio. 17 (7) (1991) 653-666.

Tables

Table 1. Properties of the human blood and parameters used in the simulations

Human blood		
Density, ρ (g/cm^3) [33] [a]		1.325
Thermal Conductivity, K_b (W/m K)[33] [a]		0.52
Specific heat, C_p (kJ/kg K) [33] [a]		3.75
Sound velocity, C_m (m/s) [34] [a]		1,603
Simulation parameters		
Computational cell size (nm^3)	100 x 100 x 100	300 x 100 x 100
Aspect ratio, L/D	40	120
Number of walkers	90,000	90,000
Time increment, Δt (ns)	0.0025	0.0025
SWNT diameter, D (nm)	2.40	2.40
Thermal equilibrium value, C_f	0.25	0.25

[a] The data here is the average of previous works [33,34].

Table 2. Ratio of effective thermal conductivity of SWNTs-in-blood divided by the thermal conductivity of pure blood with constant heat flux and different SWNT length. Thermal boundary resistances are employed from those for water suspension.

Weight fraction of SWNTs [wt%]	No. of SWNTs	**L/D = 40**		**L/D = 120**	
		Thermal boundary resistance, R_{bd} [10^{-7}, m^2K/W] (Thermal boundary conductance, K_{bd} [MW/m^2K])		Thermal boundary resistance, R_{bd} [10^{-7}, m^2K/W] (Thermal boundary conductance, K_{bd} [MW/m^2K])	
		2.0 (5)	0.84 (12)	2.0 (5)	0.84 (12)
		Probability $f_{b\text{-}CN}$		Probability $f_{b\text{-}CN}$	
		0.0025	0.006	0.0025	0.006
SWNTs perpendicular to the direction of heat flux					
0.050	31	0.971	0.970	1.001	0.999
0.075	46	0.957	0.958	1.000	0.998
0.100	60	0.940	0.943	0.993	0.998
		Random orientation		Quasi-random orientation	
0.050	31	0.988	1.003	1.096	1.217
0.075	46	0.982	1.004	1.133	1.307
0.100	60	0.977	1.006	1.170	1.371
SWNTs parallel to the direction of heat flux					
0.050	31	1.021	1.073	1.102	1.240
0.075	46	1.032	1.109	1.144	1.342
0.100	60	1.042	1.143	1.189	1.422

Table 3. Ratio of effective thermal conductivity of SWNTs-in-blood divided by the thermal conductivity of pure blood with constant heat flux and different SWNT length. Systematic study for smaller thermal boundary resistances and higher weight fraction of SWNTs.

Weight fraction of SWNTs [wt%]	No. of SWNTs	**L/D = 40**				**L/D = 120**			
		Thermal boundary resistance, R_{bd} [10^{-7}, m^2K/W] (Thermal boundary conductance, K_{bd} [MW/m^2K])				Thermal boundary resistance, R_{bd} [10^{-7}, m^2K/W] (Thermal boundary conductance, K_{bd} [MW/m^2K])			
		0.250 (40)	0.025 (400)	0.010 (1000)	0.005 (2000)	0.250 (40)	0.025 (400)	0.010 (1000)	0.005 (2000)
		Probability $f_{b\text{-}CN}$				Probability $f_{b\text{-}CN}$			
		0.02	0.20	0.50	1.00	0.02	0.20	0.50	1.00
SWNTs perpendicular to the direction of heat flux									
0.10	60	0.94	0.97	0.90	1.02	0.99	1.00	1.00	1.00
0.50	275	0.79	0.87	0.97	1.10	0.76	0.85	0.96	1.10
1.00	495	0.66	0.77	0.94	1.19	0.62	0.74	0.93	1.21
		Random orientation				Quasi-random orientation			
0.10	60	1.10	1.72	2.07	2.29	1.87	3.46	4.12	4.48
0.50	275	1.37	2.94	3.77	4.30	2.90	5.68	7.06	7.92
1.00	495	1.57	3.62	4.79	5.53	3.41	6.84	8.57	9.70
SWNTs parallel to the direction of heat flux									
0.10	60	1.49	3.51	4.72	5.53	2.16	4.84	6.26	7.15
0.50	275	2.59	7.22	10.14	12.41	3.74	9.31	12.76	15.08
1.00	495	3.13	8.90	12.78	15.77	4.46	11.37	15.83	19.01

Figure Captions

Figure 1. (a) An illustration of a cancerous cell with SWNT attached to the surface. (not to scale). Realistically, there will also be SWNTs in the fluid medium between cells as well as some attached to healthy cells. (b) A model of 60 SWNTs in the blood. The SWNT-blood system shown here is a realization of the case of randomly-oriented SWNTs with a weight fraction 0.10% and L/D = 40.0.

Figure 2. Effective thermal conductivities of differently-oriented SWNTs as a function of weight fraction of SWNTs at (a) L/D = 40 and (b) L/D = 120. The thermal boundary resistance is assumed to be equal to that of water. For each value of thermal boundary resistance and weight fraction of SWNTs, the thermal conductivity is the average of three simulation runs with different random distributions of SWNT locations. The L/D = 40 SWNTs are allowed to be oriented within 90^o of the horizontal axis (Random), and the L/D = 120 SWNTs are allowed to be oriented within 30^o of the horizontal axis (Quasi-random).

Figure 3. Dependence of effective thermal conductivities of randomly or quasi-randomly dispersed SWNTs on thermal boundary conductance. Weight fraction of SWNTs is 0.1 wt %. Orientation of SWNTs are random for $L/D = 40$ and quasi-random for $L/D = 120$.

Figure 4. Effective thermal conductivities of differently-oriented SWNTs as a function of weight fraction of SWNTs at (a) L/D = 40 and (b) L/D = 120. Relatively small thermal boundary resistance and higher weight fraction of SWNTs were examined. For each value of thermal boundary resistance and weight fraction of SWNTs, the thermal conductivity is the average of three simulation runs with different random distributions of SWNT locations. The L/D = 40 SWNTs are allowed to be oriented within 90^o of the horizontal axis (Random), and the L/D = 120 SWNTs are allowed to be oriented within 30^o of the horizontal axis (Quasi-random).

Figure 5. Effective thermal conductivities of randomly or quasi-randomly dispersed SWNTs as a function of weight fraction of SWNTs at different L/D ratios. Orientation of SWNTs are random for L/D = 40 and quasi-random for L/D = 120. For each value of thermal boundary resistance and weight fraction of SWNTs, the thermal conductivity is the average of three simulation runs with different random distributions of SWNT locations.

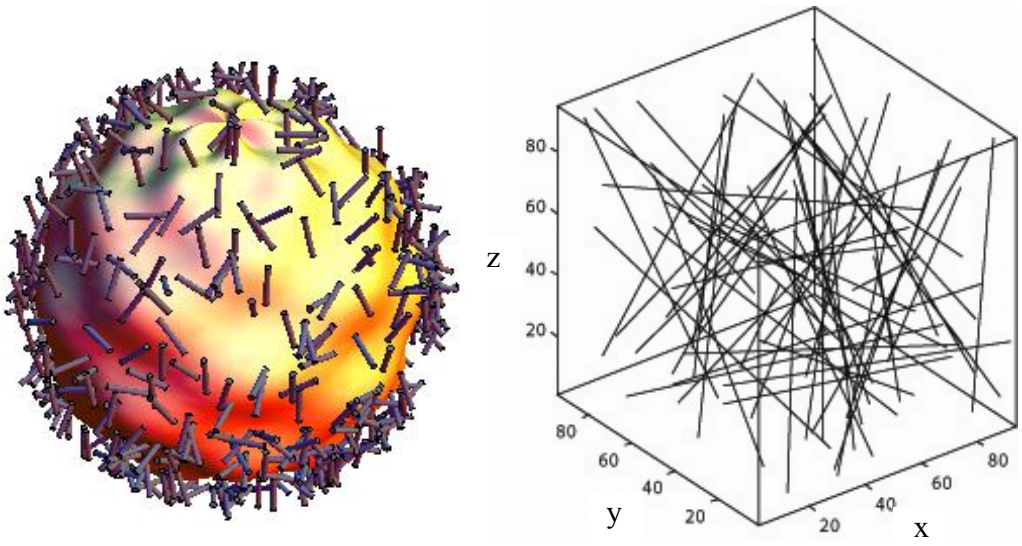

Fig. 1

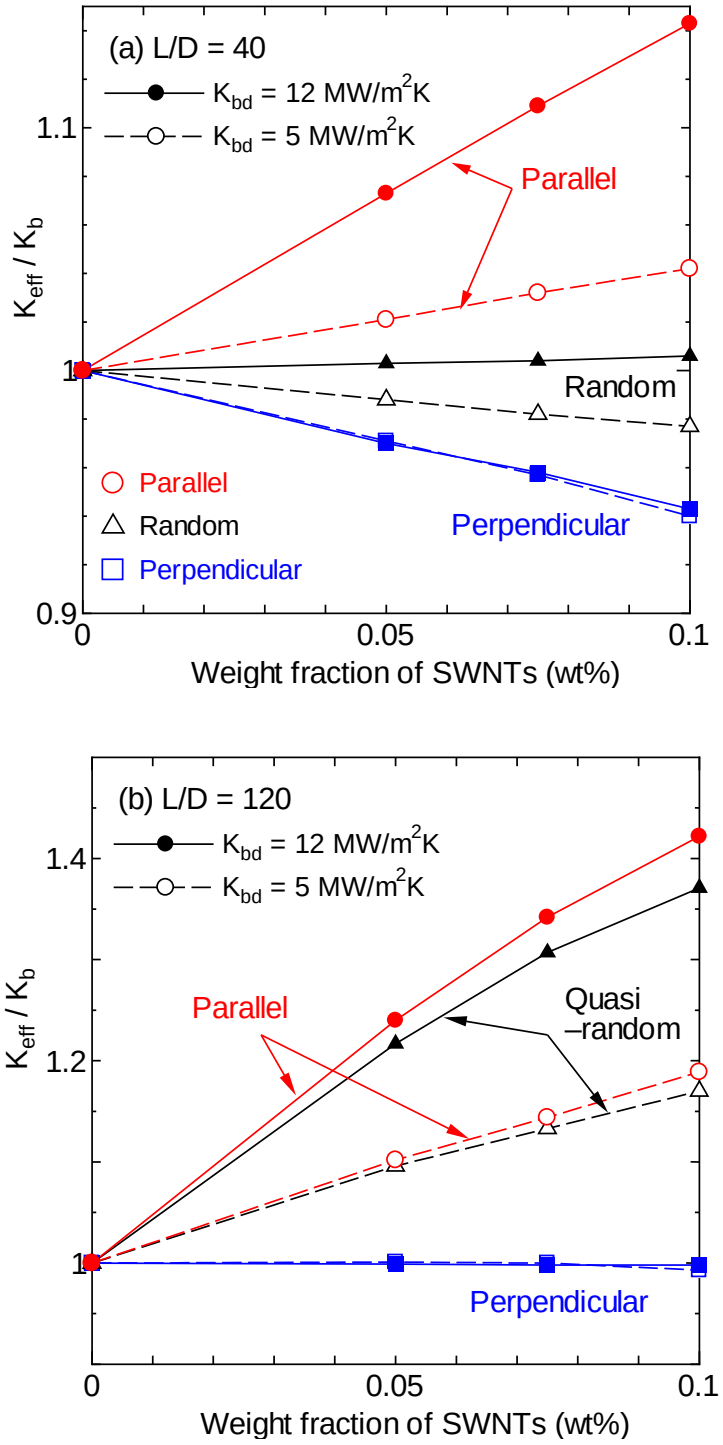
(a) L/D = 40
K_{bd} = 12 MW/m^{2}K
K_{bd} = 5 MW/m^{2}K
Parallel
Random
Perpendicular
K_{eff} / K_b
1.1
1
0.9
0
0.05
0.1
Weight fraction of SWNTs (wt%)
(b) L/D = 120
K_{bd} = 12 MW/m^{2}K
K_{bd} = 5 MW/m^{2}K
Parallel
Quasi
–random
Perpendicular
K_{eff} / K_b
1.4
1.2
1
0
0.05
0.1
Weight fraction of SWNTs (wt%)

Fig. 2

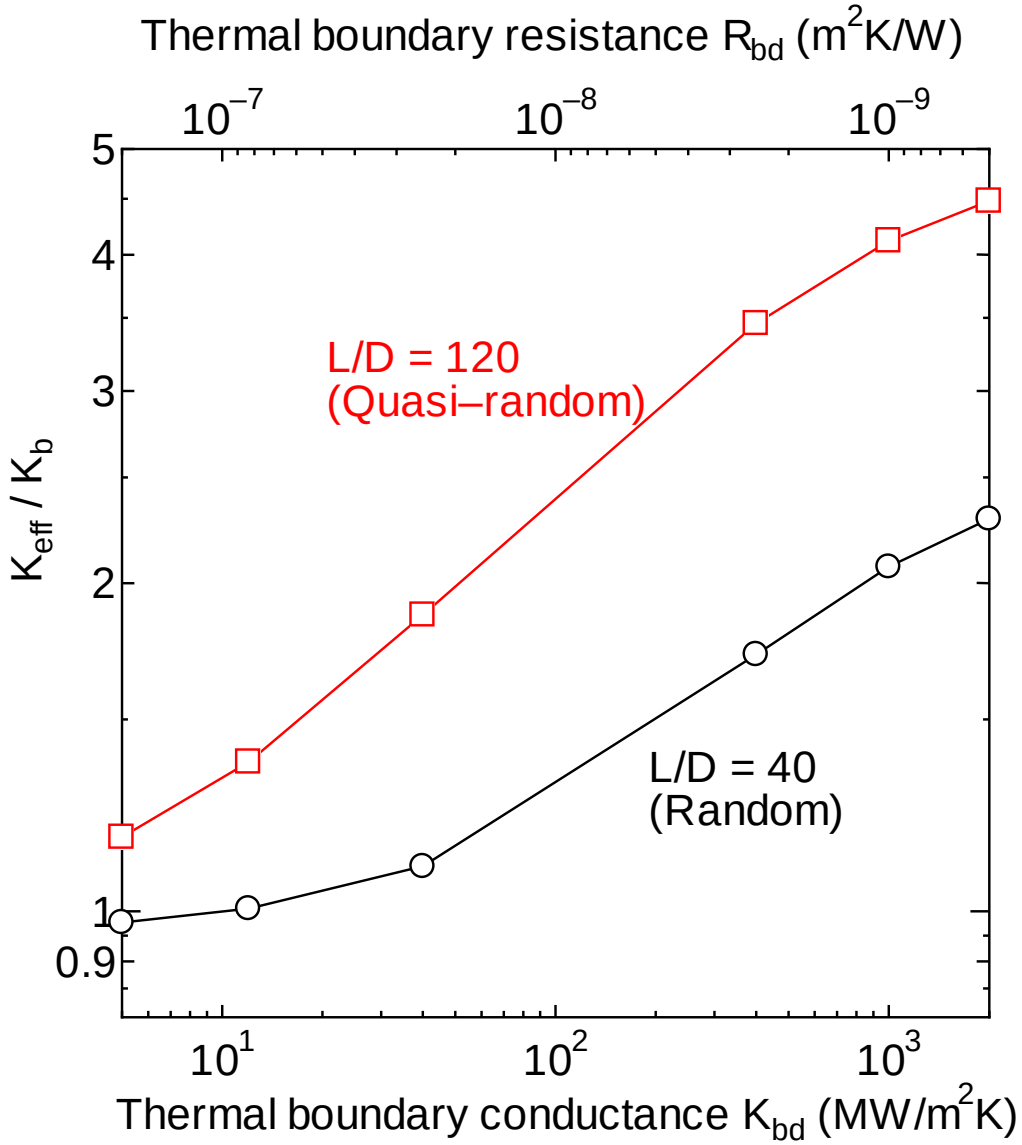
Thermal boundary resistance R_{bd} (m^2K/W)
10^{-7}
10^{-8}
10^{-9}
5
4
3
2
1
0.9
K_{eff} / K_b
L/D = 120
(Quasi–random)
L/D = 40
(Random)
10^1
10^2
10^3
Thermal boundary conductance K_{bd} (MW/m^2K)

Fig. 3

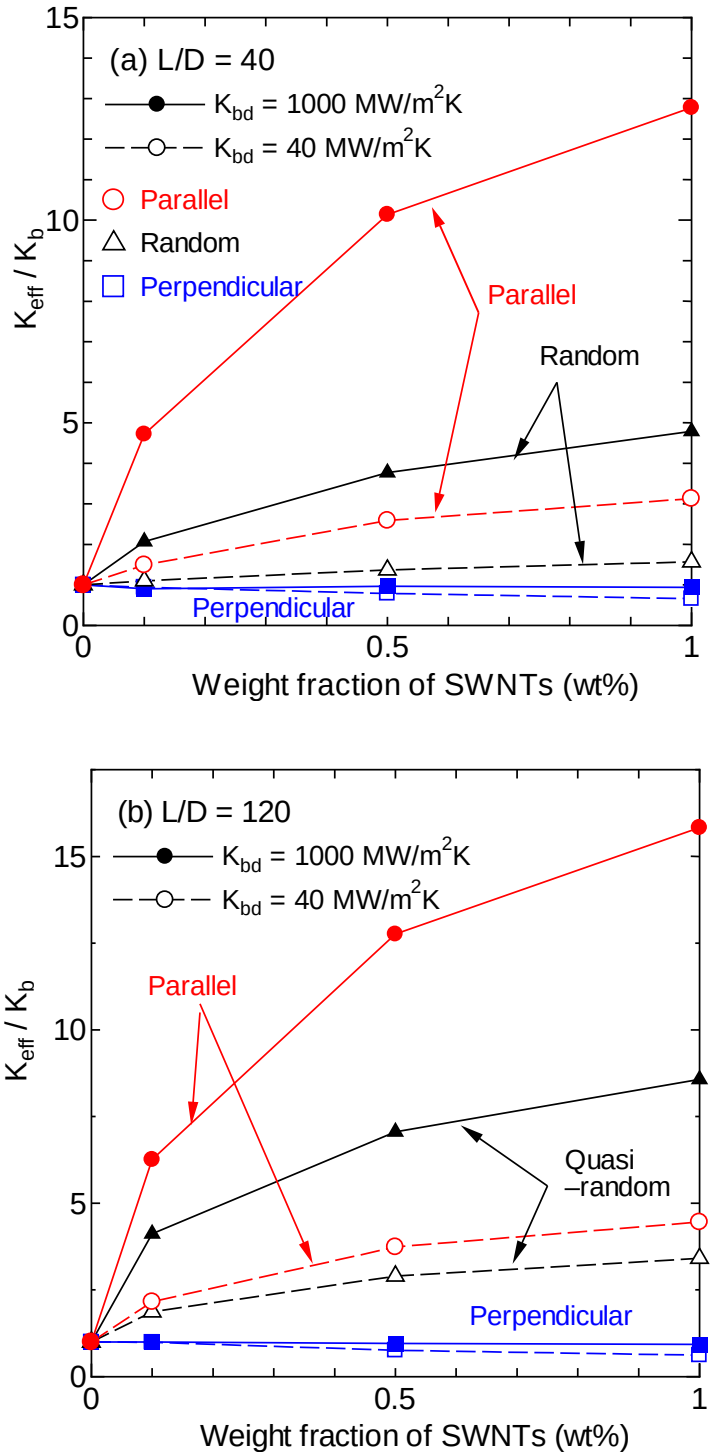
(a) L/D = 40
K_{bd} = 1000 MW/m^{2}K
K_{bd} = 40 MW/m^{2}K
Parallel
Random
Perpendicular
K_{eff} / K_b
Weight fraction of SWNTs (wt%)
(b) L/D = 120
Quasi –random

Fig. 4

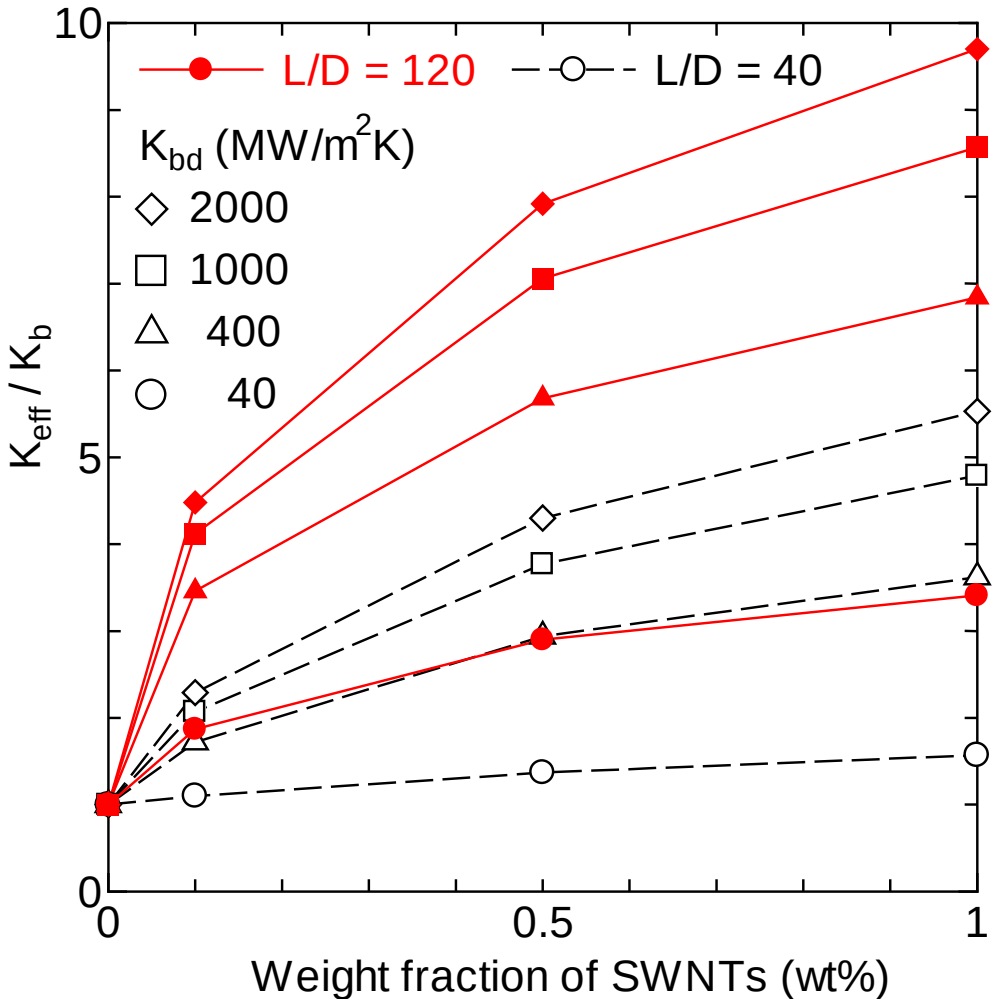
10
5
0
0
0.5
1
L/D = 120
L/D = 40
K_bd (MW/m^2K)
2000
1000
400
40
K_eff / K_b
Weight fraction of SWNTs (wt%)

Fig. 5